Reflection hologram solar spectrum-splitting filters

Deming Zhang[*a], Michael Gordon[b], Juan M. Russo[a], Shelby Vorndran[b], Matthew Escarra[c], Harry Atwater[c] and Raymond K. Kostuk[a,b]

[a]Electrical and Computer Engineering Dept., University of Arizona, 1230 E Speedway Blvd., Tucson, AZ USA 85721; [b]College of Optical Sciences, University of Arizona, 1630 E University Blvd., Tucson, AZ USA 85721; [c]California Institute of Technology, Pasadena, CA USA

ABSTRACT

In this paper we investigate the use of holographic filters in solar spectrum splitting applications. Photovoltaic (PV) systems utilizing spectrum splitting have higher theoretical conversion efficiency than single bandgap cell modules. Dichroic band-rejection filters have been used for spectrum splitting applications with some success however these filters are limited to spectral control at fixed reflection angles. Reflection holographic filters are fabricated by recording interference pattern of two coherent beams at arbitrary construction angles. This feature can be used to control the angles over which spectral selectivity is obtained. In addition focusing wavefronts can also be used to increase functionality in the filter. Holograms fabricated in dichromated gelatin (DCG) have the benefit of light weight, low scattering and absorption losses. In addition, reflection holograms recorded in the Lippmann configuration have been shown to produce strong chirping as a result of wet processing. Chirping broadens the filter rejection bandwidth both spectrally and angularly. It can be tuned to achieve spectral bandwidth suitable for spectrum splitting applications. We explore different DCG film fabrication and processing parameters to improve the optical performance of the filter. The diffraction efficiency bandwidth and scattering losses are optimized by changing the exposure energy, isopropanol dehydration bath temperature and hardening bath duration. A holographic spectrum-splitting PV module is proposed with Gallium Arsenide (GaAs) and silicon (Si) PV cells with efficiency of 25.1% and 19.7% respectively. The calculated conversion efficiency with a prototype hologram is 27.94% which is 93.94% compared to the ideal spectrum-splitting efficiency of 29.74%.

Keywords: Solar energy, photovoltaic, holographic optical elements, spectrum-splitting

1. INTRODUCTION

In order to achieve high efficiency, multi-junction solar cells require lattice-matching [1] and high quality growth techniques. The current output of the entire tandem is limited by the lowest current of all the junctions. Top cell thinning is used to reduce the current-mismatch [2] however it also introduces spectral mismatch for some of the light due to incomplete absorption.

Spectrum-splitting approach employs optics to separate different spectral components onto band-gap matched junctions [1, 3-13]. This expands the selection of materials and makes it possible to use less complicated PV cell fabrication techniques. Because the junctions do not require series connection, each junction can be optimized towards full absorption of a spectral band. Electrical isolation of the junctions also translates to higher tolerance to the incident spectrum changes. In addition, light-trapping can be incorporated on each junction through surface modifications and adding ultra-trapping filters [14] without affecting the rest of the system.

Dichroic filters are commonly used in different spectrum-splitting optical system designs [1, 4, 6, 8-13]. They have advantages such as high optical efficiency, well defined reflection band and low polarization dependence. However dichroic filters are only optimized for collimated incident light. With this angular constraint the concentration ratio is limited, as seen in Fig. 1(a). Deviation from the designed angle (Fig. 1(b)) will result in shift of the reflection spectral band [11, 13]. Depositing the dichroic filter on a curved substrate [4] can improve the spectral matching to a spherical wavefront however it will result in an increase in fabrication difficulty and cost.

*dzhang@email.arizona.edu; phone 1520 621-2031; www.ece.arizona.edu/~dzhang/

High and Low Concentrator Systems for Solar Electric Applications VII, edited by Kaitlyn VanSant, Adam P. Plesniak,
Proc. of SPIE Vol. 8468, 846807 · © 2012 SPIE · CCC code: 0277-786/12/$18 · doi: 10.1117/12.929187

Downloaded From: http://proceedings.spiedigitallibrary.org/ on 10/18/2016 Terms of Use: http://spiedigitallibrary.org/ss/termsofuse.aspx

Holographic filters are fabricated with recording the interference patterns of two or more coherent beams. It is possible to use converging or diverging reference and object wavefronts to record grating fringes matched to a focusing beam from the concentrator optics. The hologram construction geometry is shown in Fig. 2. With this configuration the holographic filter can maintain a more stable spectral rejection property for a wide-angle cone of light. As a result the concentration ratio of the system is improved.

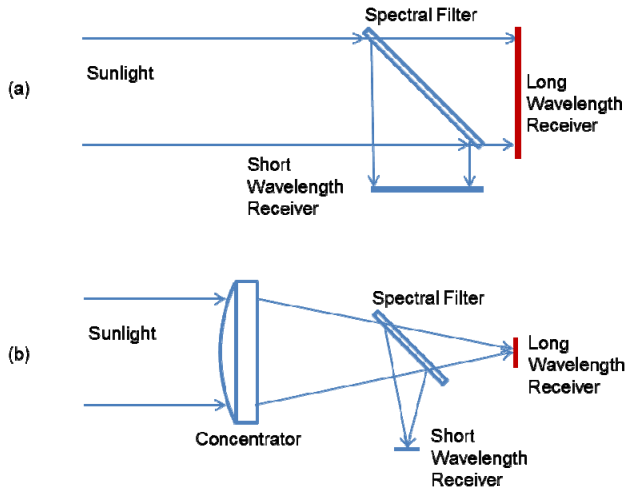

Fig. 1 Spectrum-splitting optical system geometry: (a) collimated light with no concentration; (b) focusing light with concentration.

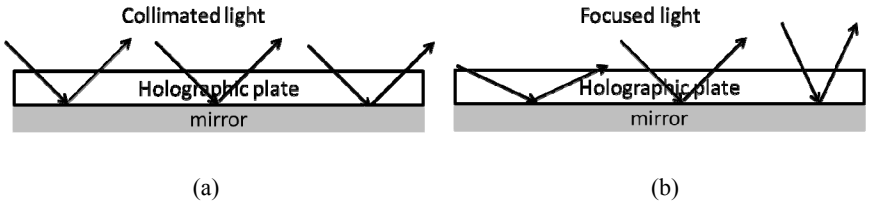

Fig. 2 Hologram construction geometries using: (a) collimated and (b) focused coherent light sources. The reference beam is reflected from the incident object beam resulting in greater interference fringe stability.

2. FABRICATION AND PROPERTIES OF DCG REFLECTION HOLOGRAMS

As spectrum-splitting filters, the volume reflection holograms need high diffraction efficiency over a broad spectral range. In addition they must have high diffraction efficiency within a designed wavelength band for a large range of incident angles and high transmittance for other wavelength. The diffraction efficiency of the hologram is defined as the ratio of the diffracted optical power $I_{dif}(\lambda,\theta)$ and the incident optical power $I_{inc}(\lambda,\theta)$.

Sensitized DCG holograms exhibit high refractive index modulation on the order of 0.1, low scattering and absorption losses [15-17]. For the unslanted reflection construction configuration in Fig. 2, it has been experimentally seen that it is possible to chirp or vary the grating period as a function of thickness [16, 17]. The grating chirp increases the spectral and angular bandwidth of the grating [16, 17]. In addition, once sealed in a water resistant encapsulation, they have excellent long-term stability.

A number of coating techniques can be used to coat sensitized gelatin layer on glass and polymer substrates. In our lab a sensitized gelatin solution was mold-coated onto glass substrates. The sensitized gelatin mixture consists of 10% gelatin solution in de-ionized water, and is sensitized with 2% ammonium dichromate by weight to water. An approximately 4 mL of sensitized gelatin solution was applied at 40°C onto the glass substrate which has spacers placed on the sides. A glass cover sheet was placed on top of the coated substrate to complete the mold. The cover sheet was coated with

Downloaded From: http://proceedings.spiedigitallibrary.org/ on 10/18/2016 Terms of Use: http://spiedigitallibrary.org/ss/termsofuse.aspx

hydrophobic release agent prior to the mold-coating process. Clips are placed on the edges of the completed mold. The sensitized gelatin solution within the mold was allowed to gelatinize in a 5°C environment for 10 minutes. After gelatinization the cover sheet can be removed and the coated substrate was allowed to dry for two hours in a constant airflow at 25°C and 45% relative humidity.

The exposure setups are shown in Fig. 3. A single input beam generates the reference beam and the object beam. This results in great stability of the interference fringes during the recording exposure. The interference fringes in the grating medium are parallel to the hologram surface. The grating period which is the spacing between the interference fringes can be changed with the input beam angle (Fig. 3 (a)). A large input beam angle corresponds to a large grating period. Input angles larger than the critical angle can be achieved with coupling via a prism, as shown in Fig. 3(b).

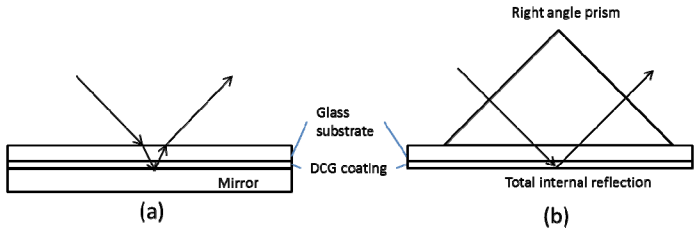

Fig. 3 Hologram construction setups with and without prism coupling.

3. OPTIMIZATION OF THE EXPOSURE AND PROCESSING PROCEDURES

Desirable optical properties for high efficiency spectrum-splitting holograms include high diffraction efficiency, large bandwidth, high transmittance for non-diffracted wavelength, low side lobes and low high-order harmonics. These optical properties require optimization of the exposure and developing procedures. The effects of exposure density, isopropanol (IPA) bath temperature, hardening bath time and layer thickness are explored experimentally.

3.1 Effect on reflection bandwidth

Experiments are done with the exposure energy varying from 0.5 second to 20 seconds while keeping the optical power on the hologram at 28mW/cm^2. Parameters in the developing process are also examined. The hardening time is varied from 2 minutes to 10 minutes and the isopropanol bath temperature is changed from 35°C to 70°C.

The transmittance of the resulting holograms is measured with an Ocean Optics USB2000+ fiber spectrometer. The diffraction efficiency is $DE(\theta) = 1 - T(\theta) - E(\theta)$ in which $T(\theta)$ is the transmittance and $E(\theta)$ is the background extinction of the gelatin and the substrate. The extinction losses include absorption and scattering.

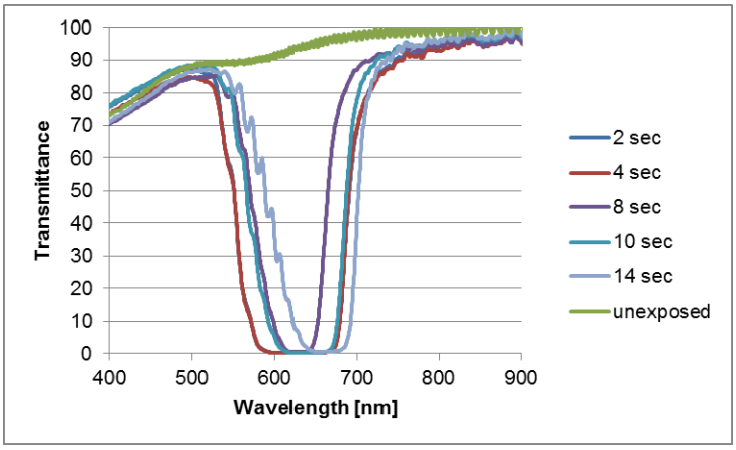

Fig. 4 Transmittance of holograms with 2 seconds to 14 seconds exposure time. (color online)

Downloaded From: http://proceedings.spiedigitallibrary.org/ on 10/18/2016 Terms of Use: http://spiedigitallibrary.org/ss/termsofuse.aspx

The transmittance curves are shown in Fig. 4 for the set of holograms developed with 5 min hardening time and 70°C isopropanol final dehydration bath. With a longer exposure time, the decrease of transmittance near 620 nm is caused by more intense diffraction.

The bandwidth of the diffraction efficiency for different hardening bath duration is shown in Fig. 5. Longer exposure time usually results in a stronger diffraction band except in the 3 sec - 7 sec range. Less hardening time gives higher bandwidth for all cases. The largest bandwidth was achieved at 10 seconds exposure for all hardening bath time. The maximum bandwidth was 160 nm with 2 minutes hardening bath.

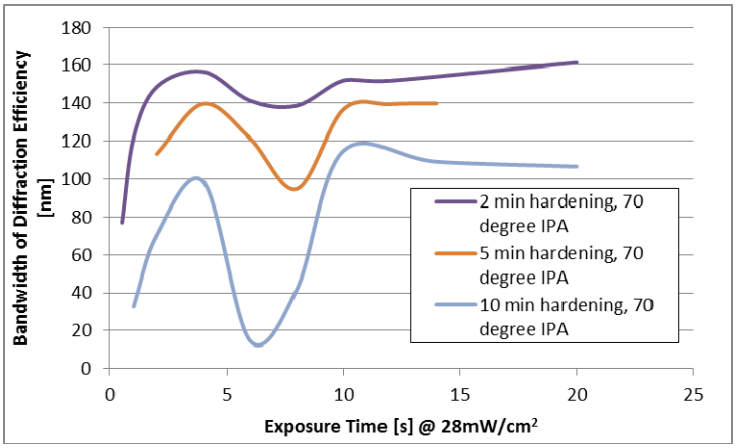

Fig. 5 Hologram diffraction efficiency bandwidth for different exposure and hardening time. (color online)

3.2 Effect on scattering

The high bandwidth associated with low hardening time comes with a trade-off of higher scattering losses. The scattering losses are measured at both 400 nm and 900 nm wavelength. At both wavelength the transmittance reductions are primarily caused by scattering losses. As seen in Fig. 6, the scattering at 900 nm wavelength is lower than 5% and it is slightly affected when the hardening bath time is decreased past 5 minutes. The scattering losses at the 400 nm wavelength are more severly affected by the hardening time. The minimum transmittance is around 73% when the hardening time is 2 minutes and the highest transmittance is 83% when the hologram is hardened for 10 minutes.

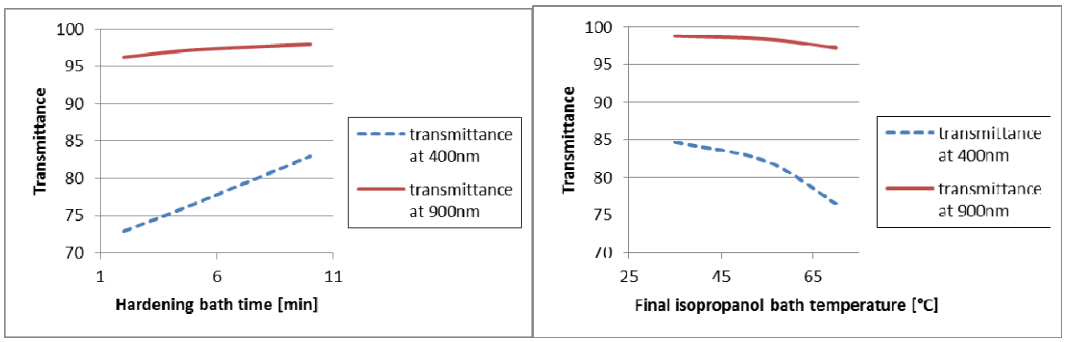

(a) (b)

Fig. 6 Transmittance reduction caused by scattering for different hardening bath time and isopropanol bath temperature measured at 400 nm and 900 nm wavelength.

The final isopropanol dehydration bath temperature also has a strong influence on scattering. As seen in Fig. 6 the scattering is relatively low for 35°C and 55°C bath but much higher for 70°C bath. This indicates that if high overall transmission and low scattering is desired, a low isopropanol bath temperature and long hardening bath should be used.

Downloaded From: http://proceedings.spiedigitallibrary.org/ on 10/18/2016 Terms of Use: http://spiedigitallibrary.org/ss/termsofuse.aspx

The scattering loss in the hologram has a λ^{-4} dependence as shown in the curve-fitting result in Fig. 7. The Rayleigh scattering behavior indicate that the scattering is caused by particles much smaller than the wavelength of visible light. This behavior agrees with earlier research that suggested the index modulation of DCG is a result of density variation of small air voids [18-20]. The transmittance dip near 570 nm is treated as outliar and is excluded from curve-fitting. It is possible that such a dip is caused by absorption (<4%) from the residual fixer in the thick gelatin layers.

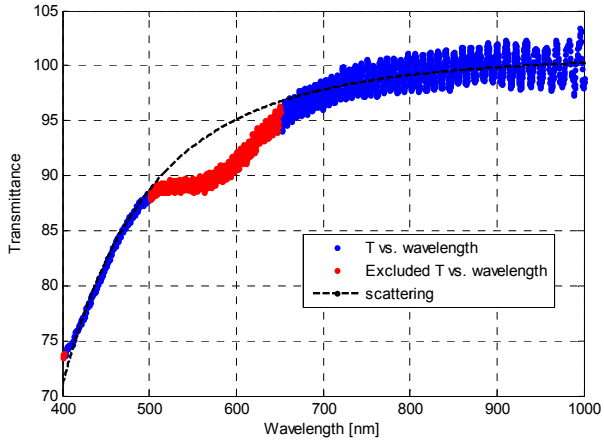

Fig. 7 Curve fitting of typical scattering chracteristics.

3.3 Fast transition between high reflection and high transmission bands

It has been observed that with a higher hologram thickness the diffraction efficiency curve more resembles a square-wave shape. It can be seen in Fig. 8 that higher gelatin concentration in the coating solution, i.e. higher gelatin layer thickness provides faster transition behavior between high reflection and high transmission bands. Both holograms are processed through the same exposure and developing procedure (70°C isopropanol bath, 5 minutes hardening and 6 seconds exposure).

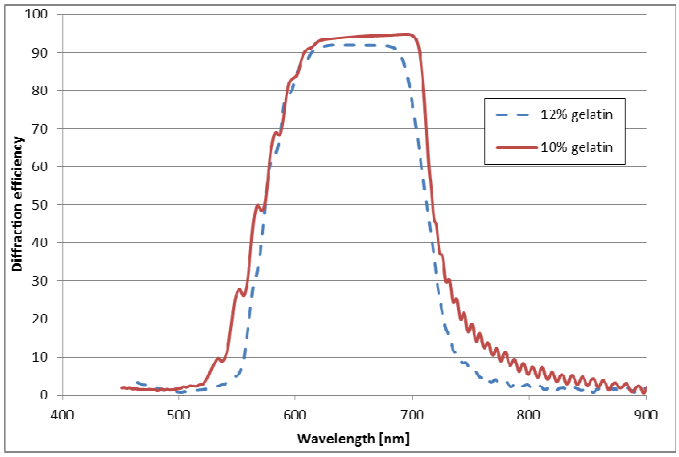

Fig. 8 Diffraction efficiency characteristics for different gelatin thickness.

4. DIFFRACTION EFFICIENCY WITH DIFFERENT ANGLE OF INCIDENCE AND POLARIZATION

In spectrum-splitting applications, optical concentration is usually needed to boost PV cell efficiency and reduce PV cell cost. As dictated by the conservation of étendue, the cone angle of incoming light at the PV cell increases with the

Downloaded From: http://proceedings.spiedigitallibrary.org/ on 10/18/2016 Terms of Use: http://spiedigitallibrary.org/ss/termsofuse.aspx

concentration ratio (Fig. 1(b)). The spectrum-splitting filters should have the ability to diffract a range of incidence angles.

The diffraction efficiency curves at 0°, 20° and 45° angles of incidence are shown in Fig. 9. Blue-shift of the central wavelength is observed for both polarizations and both filter types when the angle of incidence is increased from 0° to 45°. A shift from 900 nm to 810 nm occurs in central wavelength for the holographic filter (Fig. 9(a), (b)). A similar 10% blue-shift is seen on the dichroic filter (Fig. 9(c), (d)). This blue shift is predicted by the Bragg matching condition and it can be compensated for the holograms with focusing construction geometry as shown in Fig. 2(b). The bandwidth of the dichroic filter is weakly dependent on the incident light polarization. However the rejection bandwidth of the hologram is influenced by the polarization. It can be seen in Fig. 9(b) that the bandwidth of the TM polarization has a 17% reduction at 45° angle of incidence compared to that of the TE polarization at 45°.

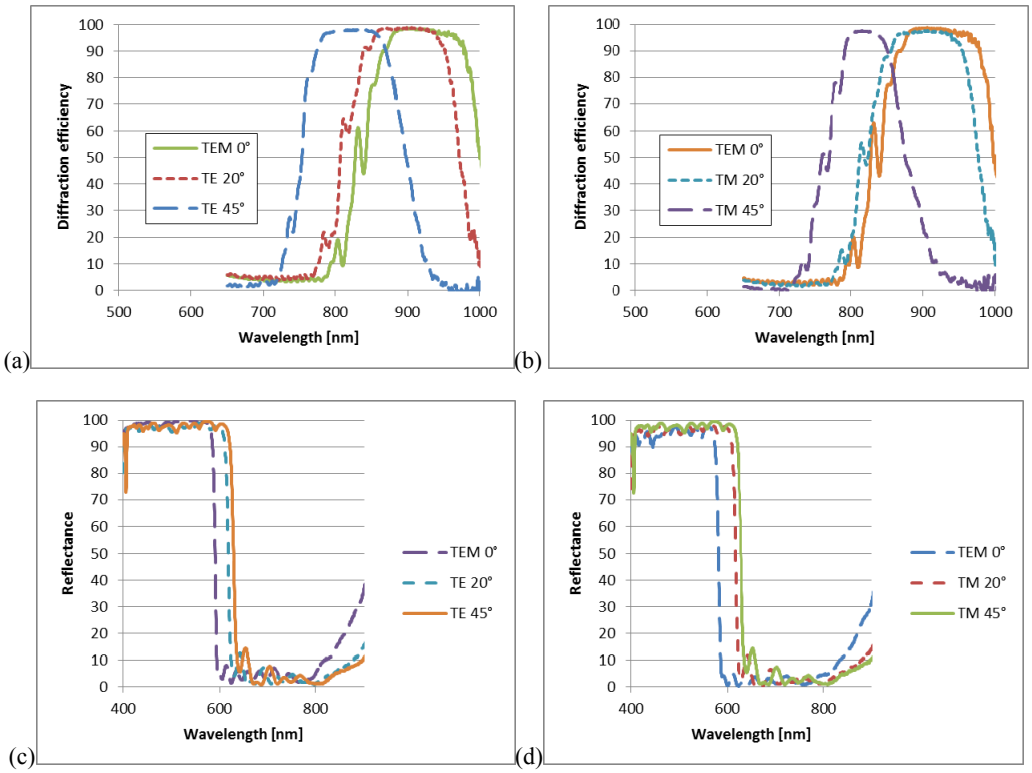

Fig. 9 Rejection bands for TE and TM polarizations at 0°, 20° and 45° in air: (a) hologram TE polarization; (b) hologram TM polarization; (c) dichroic filter TE polarization; (d) dichroic filter TM polarization.

5. DESIGN AND SIMULATION OF A GALLIUM ARSENIDE/SILICON SPECTRUM-SPLITTING PV MODULE

Recently it has been reported that epitaxial lift-off techniques can produce high quality thin-film GaAs cells with efficiency near 26% [21]. The GaAs thin-film cell absorbs light with $\lambda<875$nm. Silicon solar cells can be used to extend the absorption spectrum further to at least 1050 nm [5]. The thin-film GaAs and Si cell combination is not compatible with traditional tandem-junction approach due to large differences in lattice constants. However a single spectrum-splitting filter can combine GaAs with Si junctions. The filter with the diffraction efficiency characteristics shown in Fig. 10 is recorded on a 50 μm thick DCG hologram. The hologram reflects light between 875nm and 1025 nm towards the silicon junction. The secondary harmonic at near 480nm is caused by the non-linear behavior in the DCG sensitivity [18, 22]. The secondary order can be minimized by reducing the exposure time. However reduced exposure leads to a reduced bandwidth and diffraction efficiency in the primary diffraction order. In the case with GaAs/Si combination, both junctions have similar efficiency for the spectral range between 460nm and 510 nm, therefore the secondary order is not introducing significant loss.

Downloaded From: http://proceedings.spiedigitallibrary.org/ on 10/18/2016 Terms of Use: http://spiedigitallibrary.org/ss/termsofuse.aspx

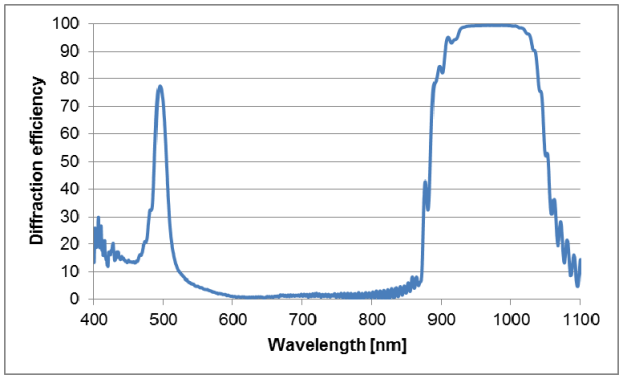

Fig. 10 Diffraction efficiency characteristics of the spectrum-splitting hologram for GaAs and Si combinaion.

The light generated current of a PV cell can be determined by its spectral responsivity $SR(\lambda)$ and the spectrum optical flux $\Phi(\lambda)$ illuminating the cell:

$$I_L = \int_{\lambda} SR(\lambda) \cdot \Phi(\lambda) d\lambda \tag{1}$$

The spectral responsivity is calculated from the external quantum efficiency with:

$$SR(\lambda) = \frac{q\lambda}{hc} EQE(\lambda) \tag{2}$$

The external quantum efficiency curves for GaAs and Si PV cells are taken from references [21, 23] and shown in Fig. 11(a).

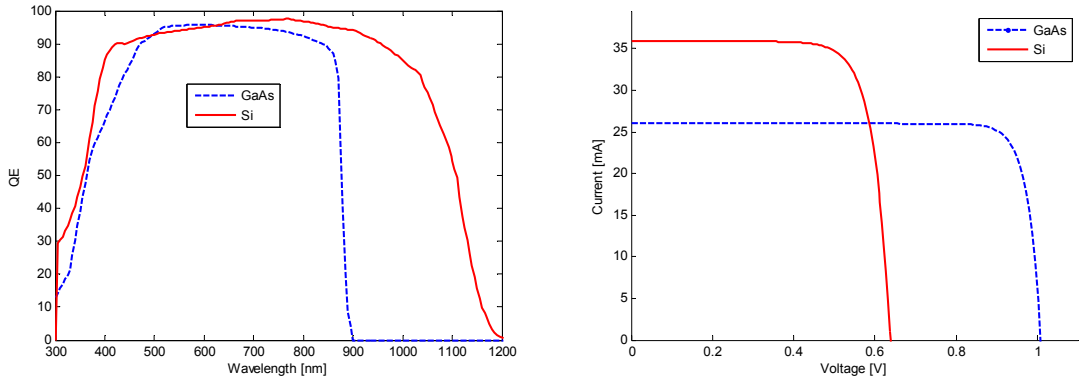

(a) (b)

Fig. 11 Quantum efficiency and IV curves of GaAs [21] and Si [23] PV cells.

The single diode equation is used to model the characteristics of a PV cell:

$$I = I_L - I_o \, \mathrm{e}^{\frac{q(V+IR_s)}{nkT}} - (V + IR_s)/R_{sh} \tag{3}$$

in which k is the Boltzmann's constant, I_o is the dark saturation current, I_L is the light generated current, n is the ideality factor, T is the device temperature in Kelvin, Rs is the series resistance and Rsh is the shunt resistance. The single diode equation assumes a constant value for the ideality factor n. The solution to the I-V function in Eq. (3) is found by using Lambert W-functions [24]. The parameters shown in Table 1 are used to compute the IV curve shown in Fig. 11(b).

The spectral conversion efficiency (SCE) is used to identify the conversion efficiency of each spectral component, it is defined as:

$$SCE(\lambda) = SR(\lambda) \cdot Voc \cdot FF \tag{4}$$

Downloaded From: http://proceedings.spiedigitallibrary.org/ on 10/18/2016 Terms of Use: http://spiedigitallibrary.org/ss/termsofuse.aspx

Table 1 IV curve parameters of Si and GaAs PV cells

PV cell	I_L [mA/cm2]	Io [A/cm^2]	n	Rs [$\Omega \cdot cm^2$]	Rsh [$\Omega \cdot cm^2$]
GaAs	26.0	2.0×10^{-16}	1.2	0.05	2×10^4
Si	36.0	2.5×10^{-9}	1.5	0.15	5000

Table 2 Electrical properties of Si and GaAs PV cells

PV cell type	Isc [mA/cm2]	Voc [V]	FF	Bandgap [eV]	One-sun efficiency (AM1.5D)
GaAs	26.0	1.01	0.85	1.424	25.1%
Si	36.0	0.64	0.77	1.1	19.7%

The spectral electrical output power is:

$$P(\lambda) = SR(\lambda) \cdot Voc \cdot FF \cdot \Phi(\lambda) \tag{5}$$

Assuming the silicon and GaAs cells have open-circuit voltages and fill-factors as listed in Table 2, the SCE of both cells are calculated with Eq. (4) and shown in Fig. 12(a).

The corresponding efficiency of each cell is obtained by:

$$\eta = \frac{\int_{\lambda} \Phi(\lambda) \cdot SCE(\lambda) d\lambda}{\int_{\lambda} \Phi(\lambda) d\lambda} \tag{6}$$

In the ideal case, the GaAs cell is treated as an ideal filter that absorbs light with λ<875 nm and transmit all other wavelength. The silicon cell receives the filtered spectrum with λ>875 nm. The combined efficiency is the sum of the efficiency of both PV cells, assuming isolated electrical connections.

For the holographic spectrum-splitting case, the hologram is modeled as a filter with the transmittance characteristics $T(\theta)$ shown in Fig. 10. The scattering is treated as purely forward and therefore no loss is introduced. The transmitted light reaches the GaAs PV cell and the reflected light reaches the Si PV cell. The concentration ratios on both cells are assumed to be 1×.

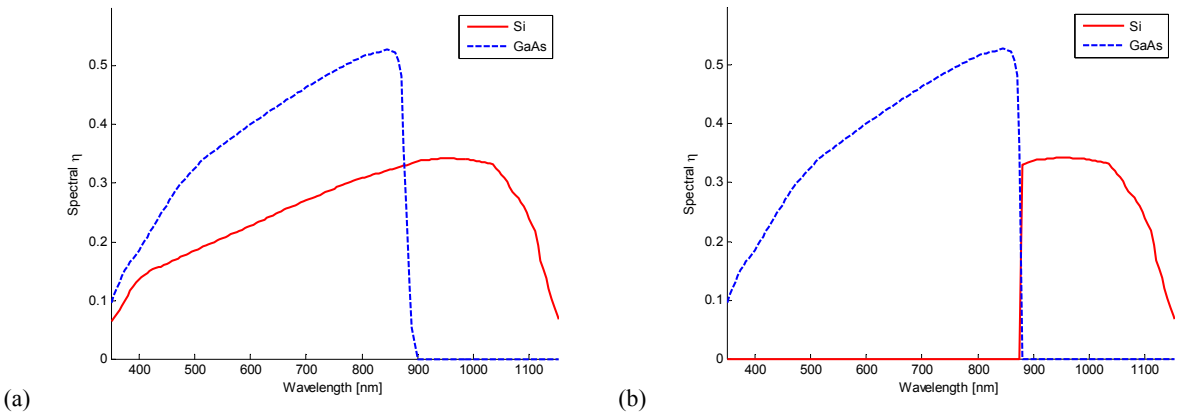

(a) (b)

Downloaded From: http://proceedings.spiedigitallibrary.org/ on 10/18/2016 Terms of Use: http://spiedigitallibrary.org/ss/termsofuse.aspx

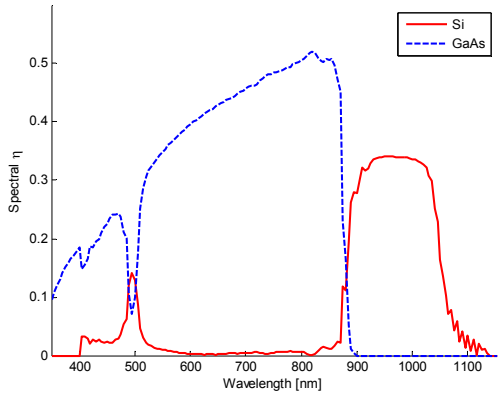

(c)

Fig. 12 Spectral conversion efficiency curves of GaAs and Si PV cells: (a) stand-alone; (b) ideal stack; (c) with prototype holographic filter

The combined efficiency is shown in Table 3 for systems with stand-alone cells, ideal filter and the prototype holographic filter. With an ideal filter, the combined efficiency is 29.74%, which is greatly improved compared to both stand-alone cells. With the prototype holographic filter, the combined efficiency is 27.94% which is 93.94% of the ideal spectrum-splitting performance.

Table 3 Efficiency of different spectrum-splitting schemes using Si and GaAs PV cells

PV cell type	Stand-alone Efficiency (AM1.5D)	Efficiency with ideal filter	Efficiency with holographic filter
GaAs	25.1%	24.69%	23.14%
Si	19.7%	5.05%	4.81%
GaAs/Si	-	29.74%	27.94%

6. CONCLUSION

Holograms fabricated in dichromated gelatin have the benefit of light weight, low scattering and absorption losses. The optical properties of reflection DCG holograms are shown to function as spectral filters in spectrum-splitting photovoltaic systems. The band-rejection DCG filter is fabricated under coherent exposure followed by wet processing. High diffraction efficiency and broad bandwidth have been achieved. In addition, it is possible to construct holograms to match converging light from concentrator optics. Rejection bandwidth of approximately 160 nm at central wavelength of 620 nm is shown with mold-coated DCG holographic plates. The effect of exposure and processing parameters on rejection bandwidth and scattering are explored experimentally. A holographic spectrum-splitting prototype is shown with Gallium Arsenide (GaAs) and silicon (Si) PV cells with efficiency of 25.1% and 19.7% respectively. The calculated conversion efficiency with a prototype hologram is 27.94% which is 93.94% compared to the ideal spectrum-splitting efficiency of 29.74%.

7. ACKNOWLEDGEMENTS

The authors wish to acknowledge support from the NSF/DOE ERC cooperative agreement No. EEC-1041895, the NSF Grant No. 0925085 and Research Corporation.

Downloaded From: http://proceedings.spiedigitallibrary.org/ on 10/18/2016 Terms of Use: http://spiedigitallibrary.org/ss/termsofuse.aspx

REFERENCES

[1] A. Barnett, D. Kirkpatrick, C. Honsberg *et al.*, "Very high efficiency solar cell modules," Progress in Photovoltaics: Research and Applications, 17(1), 75-83 (2009).

[2] D. J. Friedman, S. R. Kurtz, K. A. Bertness *et al.*, "Accelerated publication 30.2% efficient GaInP/GaAs monolithic two-terminal tandem concentrator cell," Progress in Photovoltaics: Research and Applications, 3(1), 47-50 (1995).

[3] P. Benitez, R. Mohedano, M. Buljan *et al.*, "Ultra-High Efficiency, High-Concentration PV System Based On Spectral Division Between GaInP/GaInAs/Ge And BPC Silicon Cells," AIP Conference Proceedings, 1407(1), 88-92 (2011).

[4] L. M. Fraas, J. E. Avery, H. X. Huang *et al.*, "Toward 40% and higher solar cells in a new Cassegrainian PV module," Proc. IEEE, 751-753 (2005).

[5] M. A. Green, and A. Ho-Baillie, "Forty three per cent composite split-spectrum concentrator solar cell efficiency," Progress in Photovoltaics: Research and Applications, 18(1), 42-47 (2010).

[6] J. H. Karp, and J. E. Ford, "Multiband solar concentrator using transmissive dichroic beamsplitting," Proc. SPIE, 7043, 70430F-8 (2008).

[7] C. Kerestes, W. Yi, K. Shreve *et al.*, "Transparent silicon solar cells: Design, fabrication, and analysis," Proc. IEEE, 001414-001418 (2010).

[8] B. Mitchell, G. Peharz, G. Siefer *et al.*, "Four-junction spectral beam-splitting photovoltaic receiver with high optical efficiency," Progress in Photovoltaics: Research and Applications, 19(1), 61-72 (2011).

[9] A. Mokri, and M. Emziane, "A photovoltaic system with three solar cells and a band-stop optical filter," Journal of Renewable and Sustainable Energy, 3(2), 023113-11 (2011).

[10] D. Vincenzi, A. Busato, M. Stefancich *et al.*, "Concentrating PV system based on spectral separation of solar radiation," physica status solidi (a), 206(2), 375-378 (2009).

[11] X. Wang, N. Waite, P. Murcia *et al.*, "Lateral spectrum splitting concentrator photovoltaics: direct measurement of component and submodule efficiency," Progress in Photovoltaics: Research and Applications, 20(2), 149-165 (2012).

[12] K. Xiong, S. Lu, J. Dong *et al.*, "Light-splitting photovoltaic system utilizing two dual-junction solar cells," Solar Energy, 84(12), 1975-1978 (2010).

[13] M. Buljan, P. Benitez, R. Mohedano *et al.*, "Free-form Fresnel RXI-RR Kohler design for high-concentration photovoltaics with spectrum-splitting," Proc. SPIE, 8124, 81240H-11 (2011).

[14] D. Zhang, S. Vorndran, J. M. Russo *et al.*, "Ultra light-trapping filters with broadband reflection holograms," Opt. Express, 20(13), 14260-14271 (2012).

[15] C. G. Stojanoff, O. Brasseur, S. Tropartz *et al.*, "Conceptual design and practical implementation of dichromated gelatin films as an optimal holographic recording material for large-format holograms," Proc. SPIE, 2042, 301-311 (1994).

[16] C. G. Stojanoff, J. Schulat, and M. Eich, "Bandwidth- and angle-selective holographic films for solar energy applications," Proc. SPIE, 3789, 38-49 (1999).

[17] H. Schuette, and C. G. Stojanoff, "Effects of process control and exposure energy upon the inner structure and the optical properties of volume holograms in dichromated gelatin films." Proc. SPIE, 3011, 255-266 (1997).

[18] S. Case, and R. Alferness, "Index modulation and spatial harmonic generation in dichromated gelatin films," Applied Physics A: Materials Science & Processing, 10(1), 41-51 (1976).

[19] B. J. Chang, and C. D. Leonard, "Dichromated gelatin for the fabrication of holographic optical elements," Appl. Opt., 18(14), 2407-2417 (1979).

[20] R. K. Curran, and T. A. Shankoff, "The Mechanism of Hologram Formation in Dichromated Gelatin," Appl. Opt., 9(7), 1651-1657 (1970).

[21] G. J. Bauhuis, P. Mulder, E. J. Haverkamp *et al.*, "26.1% thin-film GaAs solar cell using epitaxial lift-off," Solar Energy Materials and Solar Cells, 93(9), 1488-1491 (2009).

[22] Z. N. Kalyashova, E. V. Kalyashov, G. A. Cheremisina *et al.*, "Intensive Bragg harmonics in reflection holograms in dichromated gelatin: 1," Proc. SPIE, 3011, 279-284 (1997).

[23] J. Zhao, A. Wang, M. A. Green *et al.*, "19.8% efficient honeycomb textured multicrystalline and 24.4% monocrystalline silicon solar cells," Applied Physics Letters, 73(14), 1991-1993 (1998).

[24] A. Jain, and A. Kapoor, "Exact analytical solutions of the parameters of real solar cells using Lambert W-function," Solar Energy Materials and Solar Cells, 81(2), 269-277 (2004).

Downloaded From: http://proceedings.spiedigitallibrary.org/ on 10/18/2016 Terms of Use: http://spiedigitallibrary.org/ss/termsofuse.aspx